Vol. 17, No. 2 (2018) 389-407
Revista Mexicana de Ingeniería Química

A STUDY ON EMPIRICAL AND MECHANISTIC APPROACHES FOR MODELLING CANE SUGAR CRYSTALLIZATION

ESTUDIO DE ENFOQUES EMPÍRICOS Y MECANÍSTICOS PARA EL MODELADO DE LA CRISTALIZACIÓN DE AZÚCAR DE CAÑA

E. Bolaños-Reynoso[1]*, K. Sánchez-Sánchez[1], L. López-Zamora[1], L. Ricardez-Sandoval[2]
[1]*División de Estudios de Posgrado e Investigación, Instituto Tecnológico de Orizaba - TecNM. Oriente 9 Núm. 852 Colonia Emiliano Zapata, Orizaba, Veracruz, 94320, México.*
[2]*Deparment of Chemical Engineering, University of Waterloo, Waterloo, Ontario NL2 3G1, Canada.*
Received September 3, 2017; Accepted December 28, 2017

Abstract
This study presents the kinetic modelling for cane sugar batch crystallization. The study is based on two approaches to describe the nucleation (homogeneous primary and secondary) and growth kinetics, and the birth and death rates of crystals: a) empirical models with equations of type power law (TPL) and b) mechanistic approach with thermodynamic equations. Both approaches, describing the phenomena of crystallization at the microscopic level (by solving population balance equation by method of lines), were validated using experimental data from a pilot-scale plant. From the results of both approaches and experimental validation, we conclude that the mechanistic approach best represents the dynamic behavior of cane sugar batch crystallization under different operational conditions than the empirical approach (TPL).
Keywords: crystallization, modelling, kinetics, mechanistic and empirical approaches.

Resumen
Este estudio presenta el modelado cinético para la cristalización por lotes de azúcar de caña. El estudio se basa en dos enfoques para describir las cinéticas de nucleación (primaria homogénea y secundaria), de crecimiento y las tasas de nacimiento y muerte de cristales: a) modelos empíricos con ecuaciones de tipo ley de potencias (TLP) y b) enfoque mecanístico con ecuaciones termodinámicas. Ambos enfoques describen los fenómenos de cristalización a nivel microscópico (con la solución del balance de población por método de líneas) y fueron validados usando datos experimentales provenientes de una planta escala piloto. De los resultados de ambos enfoques y la validación experimental, se concluye que el enfoque mecanístico representa mejor los comportamientos dinámicos de la cristalización por lotes de azúcar de caña bajo diferentes condiciones operativas con respecto al enfoque empírico (TLP).
Palabras clave: cristalización, modelado, enfoque mecanístico y empírico.

1 Introduction

Batch crystallization is a separation process where molecules transfers from a solute dissolved within a liquid or gas toward a solid phase in two steps: 1) nucleation and 2) crystal growth. Process performance is often measured in terms of crystal properties at the end of the batch, e.g. crystal size distribution (CSD), which comprises the crystal average diameter (% volume D(4,3)) and the standard deviation (% volume S(4,3)), as well as the mass of crystals. Phenomena producing wide distributions in CSD such as secondary nucleation are undesirable since they generate a product with dispersed shape characteristics, resulting in unsatisfactory transport properties for downstream processing such as filtration and drying (Ouiazzane *et al*., 2008; Nagy *et al*., 2013).

The development of highly detailed mathematical models describing the nonlinear dynamic behavior of the crystallization process is critical to determine optimal operating conditions that produce high quality products, e.g. narrow CSD and specific shape (Gerstlauer *et al*., 2002, Motz *et al*., 2002). Largely, the quality of the model depends on the assumptions made during its development, the accuracy of the experimental data used for estimation of unknown kinetic parameters, and the numerical algorithm employed to solve the model equations (Motz *et al*., 2002; Mesbah *et al*., 2009). A commonly accepted

* *Corresponding author. E-mail*: eusebio.itorizaba@gmail.com
doi: 10.24275/10.24275/uam/izt/dcbi/revmexingquim/2018v17n2/Bolanos ; *issn-e*: 2395-8472

approach to describe suspensions within a crystallizer is the population balance equation (PBE), introduced by Randolph and Larson (1988). Its application generally leads to complex mathematical models involving discretization schemes of a large set of ordinary differential equations (Ramkrishna, 2000; Ma *et al*., 2002, Samad *et al*., 2013). Moreover, the crystallization modelling also requires a detailed mathematical description for the nucleation and crystal growth rates. Consequently, previous works have reported different approaches with successful applications for process improvement. Nagy *et al*., (2003) employed empirical models on the development of a control strategy that quantifies uncertainty on kinetic constants for nucleation and crystal growth for KNO_3. Bolaños *et al*., (2014) reported optimal agitation rate trajectories that maximized the average crystal diameter D(4,3) from empirical kinetic models under uncertainty for the cane sugar batch crystallization. Bensehard *et al*., (2015) studied the sensitivity of parameter estimation on empirical kinetic constants and evaluated how oversimplified model assumptions mislead the interpretation of experimental results.

While empirical models have limited predictive capabilities outside their operating range covered by the experimental data used for parameter estimation (Westhoff and Kramer, 2012), mechanistic models, i.e. models developed based on balance conservation principles, are developed based on the system physicochemical properties and geometric characteristics of the crystallization unit (i.e. thermodynamic equations). According to Bermingham *et al*., (2003), mechanistic models are required to describe crystallization processes in a wide range of operating conditions, where secondary nucleation plays a key role. Those models provide a complete description of the frequency collisions of the crystals due to agitation rate. Moreover, such modelling approach has less unknown parameters compared with the empirical models and can be obtained by a simple formulation of an optimization problem. Gerstlauer *et al*., (2002) presented the development of the mathematical model proposed by Gahn, C. & Mersmann, A., (1999a) for batch and continuous crystallization. In that model, a constant parameter related to the degree of primary nucleation heterogeneity is considered. Kalbasenka *et al*., (2011) made use of experimental data obtained from different batches to estimate the kinetic parameters and dismissed the assumption of invariability of the kinetic parameters throughout the process. Finally, Quintana *et al*., (2008) presented a first study on the analysis of two different approaches to modelling the crystallization kinetics based of an empirical power law type (TPL) equations and a mechanistic framework. That work suggested that surface-integration mechanism dominates in cane sugar crystallization.

The aim of this study is to present an analysis of the prediction capabilities for the crystallization kinetics obtained from empirical and mechanistic modelling approaches. The PBE incorporates the proposed models and solved using the method of lines. Experimental data collected from pilot-scale plant considering different agitation rates were used to validate the two modelling approaches against different operating conditions. The results will benefit future studies on modelling, optimization and real-time process control, considering the advantages and limitations of both modelling approaches for the cane sugar batch crystallization.

The structure of the article is as follows: the next section entitled Experimental set-up presents a brief description of the pilot-scale plant and instrumentation devices following by a summary of the operation strategy for the cane sugar batch crystallization. In addition, a general methodology that describes the image-based algorithm used for CSD quantification is presented in that section. The Methodology Section presents the general mathematical framework where the population balance equation (PBE) and their corresponding assumptions are considered. This section also includes the empirical and the mechanistic approaches to modelling the crystallization kinetics. The end of this section presents the parameter estimation analysis. Results and discussions section presents the simulations using both modelling approaches, with the aim to determine the accuracy of each approach. Experimental data validates the results from simulation. Finally, conclusions are presented at the end of this article.

2 Experimental set-up

2.1 Pilot-scale batch crystallizer

Figure 1 shows a schematic set-up of the pilot-scale plant batch crystallizer used in the experimental stage. A brief description of the experimental set-up is presented in Table 1, which includes a stainless steel batch crystallizer (pilot-scale plant) with a heating-

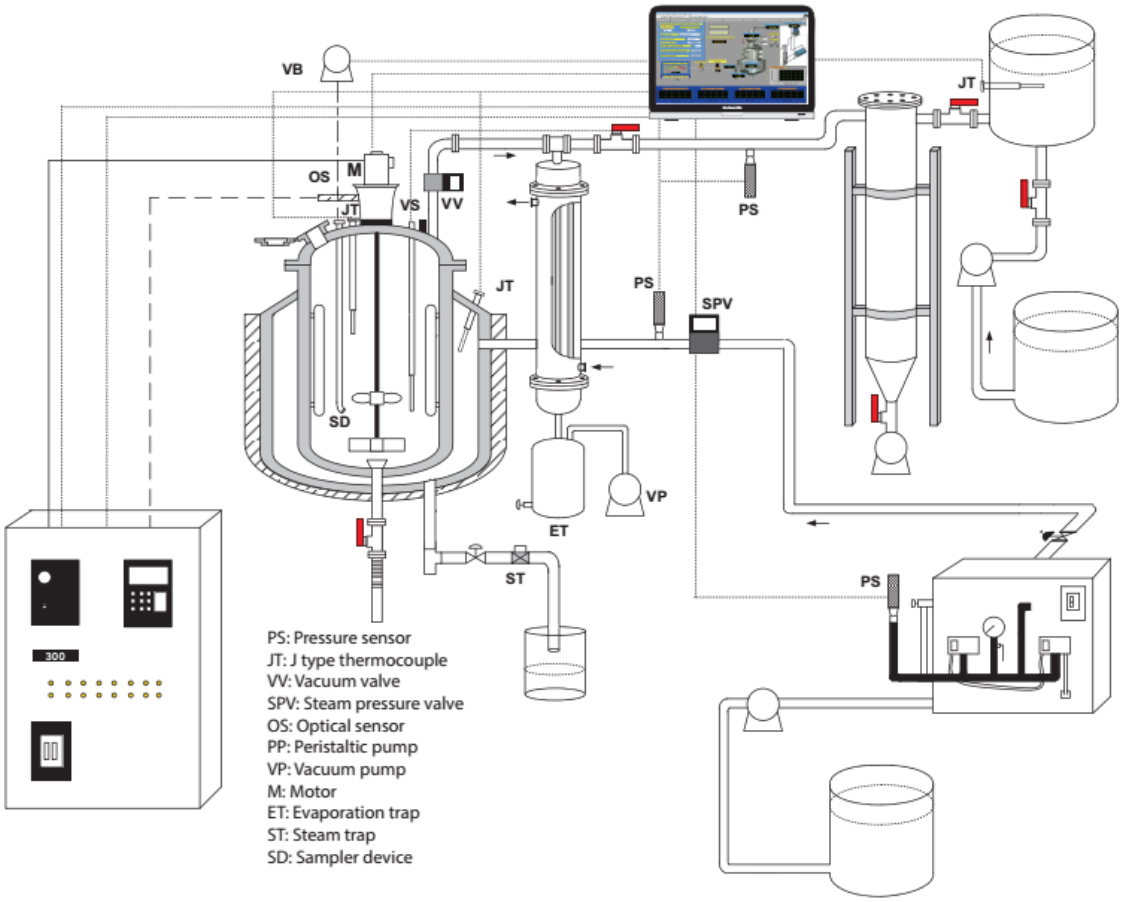

Fig. 1. Pilot-scale batch crystallization plant.

cooling jacket, steam generator, DC motor, vacuum pump, a direct contact condenser, a slurry trap and a tachometer that measure the agitation rate. The studies reported by Bolaños *et al*., (2008) and Bolaños *et al*., (2014) provide a detailed description of all the equipment and instrumentation devices installed in the actual pilot-scale plant.

The start-up begins by loading the saturated solution into the crystallizer. The solution is prepared with 6.569 kg of high purity commercial sugar and 2.528 kg of distillated water at 70 °C (density within 1.3594 - 1.3614 g/c m^3) and is kept constant during 30 minutes with an agitation rate of 300 rpm to ensure a solution free of crystals. Then, the operation begins by loading 5 grams of seed crystals (D(4,3) = 173.05 μm, S(4,3) = 18.72 μm) through a vertically sampler into the crystallizer at the fifth minute (this avoids dissolution of seed crystals). During the first stage, the vacuum pressure is set to 76.20 kPa for 40 min and then increased up to 86.66 kPa, following a cooling natural profile. Sampling is performed at every 15 minutes to obtain experimental information about concentration (in terms of density) measured in a digital densimeter (Anton Paar DMA 4500, see description in Table 1), CSD and mass of crystals. A vertically sampler device introduced into the crystallizer takes two samples of slurry (solution and crystals) of 10 ml without affecting the vacuum pressure. Finally, it is applied a centrifugation at 3,000 rpm to separate crystals from the solution.

2.2 *Image-based approach for CSD quantification*

CSD quantification from the crystals obtained on each sample applies an image-based approach as an alternative technique to laser diffraction. This approach aims to determine the CSD from the crystals obtained on each sample.

Table 1. Devices of the experimental pilot-scale batch crystallizer

Quantity	Device
1	DMA 4500 (high-resolution with 1e-05 of significant figures) density measuring module, based on the proven oscillating U-tube principle ensuring highly accurate density values.
2	J type thermocouple, temperature of 0-760 ºC, cable length 1 m.
2	Thermowells. Stainless steel.
1	Vacuum pump Felisa FE-1400, 0.3 HP.
1	Proportional control solenoid valve, Burkert. Average temperature of 140 ºC, with digital controller.
6	2-way solenoid valve, normally closed, steel, Parker.
6	Flow valve to allow water and steam flow through pipes.
1	Pressure regulator Norgren Mexico.
1	Vacuum transmitter. Cole-Parmer Model 07356-11. Stainless Steel.
2	Pressure transmitter, Cole-Parmer Model 68072-08.
1	Steam boiler, model MBA9 of SUSSMAN; maximum pressure, 100 Psi; work voltage, 240 VAC; control voltage, 120 VAC.
1	Hydraulic pump, QB60 Clean Water Pump, 1.5 HP.
1	Galvanized pipe system for water circulation.
1	High temperature insulation system.
1	Manometer, ASHCROFT.
1	Condenser, stainless steel surface.
1	Plastic tank 1100 L capacity.
1	Stainless steel crystallizer of 12.77 L, heating-cooling jacket of 11.10 L, four vertical wall baffles of 17 cm (wide) by 3.5 cm (length), agitation arrow of 39 cm (length).
1	Agitator for closed tank, model NSDB of HP, direct transmission of 1750 rpm (1 phase, 60 cycles), 110 VCA totally closed, without ventilation, stainless steel 316 with bridle of 4 in. (diameter) in stainless steel, with agitating arrow of 26 in. (length) and 1/2 in. of diameter in stainless steel 316; velocity investor (driver) integrated with rank from 0 to 1750 rpm
1	Marine propeller type impeller.
1	Programmable tachometer. Range from 50 to 999,990 rpm.
1	Optical sensor for distances of 3 ft. Range 1 -150000 rpm.
1	Microscope trinocular 48923-30 Cole-Parmer.
1	Monochrome camera with RS-170, video lens with 0.19 mm per pixel.
1	PC, Intel Pentium IV. Operating system XP, 4 GB RAM memory, hard disc of 1 TB
4	Data acquisition card (NI PCI-6023E, NI PCI-6025E, NI PCI-6711 and NI PCI-232/2). Analogic-digital and digital-analogic converters allow the input/output analogic and digital signals.
2	Signal conditioning module (NI SCC-TC02).
1	Image acquisition card (NI PCI-1409).
1	Galvanized steel condenser of direct contact with 2.27 m high and 0.3 m of diameter.

This procedure involves the image acquisitions using a microscope camera Carl Zeiss Micro Imaging GmbH with achromatic lens of 10X and the software Vision Assistant 2017 (National Instruments, Inc.). The imaging system is able to capture 10 images from the sample, which is later on processed through a threshold technique (Solomon and Breckom, 2011) to segment each individual's crystals (Velazquez *et al*., 2010).

Areas with high density of crystals are isolated, manually analyzed, and counts the black pixels areas (crystals). The imaging system compares the black pixels areas with specific standards to identify the crystals presented according to binary images (background) (Hanks, 1997). CSD quantification involves the measure of an average of 100 crystal's areas.

Furthermore, the approach uses a Neubauer's camera to count the particles and determine a conversion factor through a calibration procedure (Bolaños *et al*., 2008; Bolaños *et al*., 2014), i.e. the conversion factor enables a direct relation from one pixel (one-pixel side) to 1.074 μm (length).

3 Methodology

3.1 General mathematical framework

This section presents the mathematical models used in this study to perform the analysis of the empirical and mechanistic approaches for batch crystallization kinetics of cane sugar. The vacuum batch crystallization model involves two phases: 1) a continuous liquid phase (distillated water and dissolved cane sugar) and 2) a dispersed solid phase (cane sugar crystals). The model also considers the mass transport generated by supersaturation, which affects the primary homogeneous nucleation (n_{nu}) and crystal growth (n_{gr}) (Gestlauer *et al*., 2002). The density's number (n) describes the crystal flux number of the dispersed solid phase in equation (1), which is a function of the crystal's characteristic length L and processing time.

$$\frac{\partial n(L,t)}{\partial t} = -\frac{\partial (G(t)\cdot n(L,t))}{\partial L} + n_{nu} \pm n_{at} \tag{1}$$

Initial and boundary conditions for this system are as follows:

$$n(L,t=0) = n_{seed}(L) \tag{2}$$

$$n(L=\infty,t) = 0 \tag{3}$$

In the case of seeding, Equation (2) gives the initial condition, where $n_{seed}(L)$ specifies the CSD of the seeded crystals. Equation (3) specifies that no crystals with size $L \rightarrow \infty$ are expected and are physically infeasible.

Since the continuous liquid phase is a binary mixture of distillated water and dissolved cane sugar, the phase's dynamic behavior is described by the balance of the total number of moles n_{Liq}. Equation (4) was adapted from the equation reported by Motz *et al*. (2002) for batch crystallization. This equation assumes that solvent molecules are not adhered to each other (i.e. $a = 0$).

$$\frac{\partial n_{Liq}}{\partial t} = -(1+a)\cdot n_{nu} - (1+a)\cdot n_{gr} - n_{vap} \tag{4}$$

The evaporation rate of water as a solvent n_{vap} is calculated based on the Hertz-Knudsen equation (Marek *et al*., 2001):

$$n_{vap} = \alpha_V \left(\frac{M_w}{2\pi R T_{cr}}\right)^{1/2} (p_V - p_l) M_w \tag{5}$$

where α_V is the adhesion coefficient, p_V and p_l are the liquid phase pressure and vapor phase pressure, respectively; M_w is the molar mass and R is the ideal gas constant.

In addition, Equation (6) shows the balance of moles number for dissolved crystals $n_{Liq,A}$. Exchange fluxes n_{nu} and n_{gr} occur as development of new nuclei or crystal growth (Equations 7 and 8, respectively). Equation (9) specifies the initial conditions of state of the liquid phase in the batch.

$$\frac{\partial n_{L,A}}{\partial t} = -n_{nu} - n_{gr} \tag{6}$$

$$n_{nu} = \frac{k_v \cdot \rho_s}{M_s} \int_0^{L_\infty} L^3 \cdot \delta(L - L_0) \cdot B_{nu} \cdot V_{liq} dL \tag{7}$$

$$n_{gr} = \frac{3 \cdot k_v \cdot \rho_s}{M_s} \int_0^{L_\infty} L^2 \cdot G \cdot n(L,t) dL \tag{8}$$

$$n_{liq}(t=0) = n_{l,0}; n_{liq,A}(t=0) = n_{liq,A,0} \tag{9}$$

To complete the model of a batch crystallizer, the energy balance should be considered. this model needs to be defined in terms of the temperature inside the crystallizer T_{cr} (Equation 10) and the temperature inside the cooling jacket T_j (Equation 11).

$$Cp_{cr} \frac{dT_{cr}}{dt} = -\Delta h^*_{cr} \cdot (n_{nu} + n_{gr}) + J_{cool} \tag{10}$$

$$Cp_j \frac{dT_j}{dt} = -Cp_j^* \cdot n_{cool}(t) \cdot (T_{j,in} - T_j) - J_{cool} \quad (11)$$

where Cp_{cr} is the heat capacity within crystallizer, Δh_{cr}^* is the molar heat due to crystallization, J_{cool} is the heat exchanged with the cooling jacket. Moreover, equation (11) defines the heat transfer inside the cooling jacket; Cp_j and Cp_j^* denote the heat capacity of the coolant and the molar heat capacity at the inlet, respectively. Furthermore, equations (12) and (13) specify the initial conditions for the energy balance equations. Equation (14) describes the energy flux J_{cool} included in equations (10) and (11).

$$T_{cr}(t=0) = T_{cr,0} \quad (12)$$

$$T_j(t=0) = T_{j,0} \quad (13)$$

$$J_{cool} = -k_{cool} \cdot A_{cool}(T_{cr}) \quad (14)$$

3.2 Mechanistic kinetic modelling approach

The mathematical framework proposed by Gahn and Mersmann (1999a, 1999b) is a suitable mechanistic model for this process since it covers a wide range operating conditions. The key assumption for this model is that the process must be dominated by secondary nucleation that appears in seeded crystallizers (Kalbasenka *et al*., 2011). The model describes the kinetics for nucleation, crystal growth and attrition in terms of the physical properties of the system. In this context, equation (15) represents the primary homogeneous nucleation rate.

$$n_{nu} = 1.5 D_{AB} (C^* N_A)^{7/3} S^{7/3} \sqrt{\frac{\gamma_{CL}}{kT_{cr}}} \frac{1}{C_C N_A} \exp\left(-\frac{16\pi}{3} \left(\frac{\gamma_{CL}}{kT_{cr}} \right)^3 \left(\frac{1}{C_C N_A} \right)^2 \frac{1}{(\ln S)^2} \right) \quad (15)$$

where C^* is the saturation concentration at temperature T_{cr}, N_A is the Avogadro's number, k the Boltzman constant C_C, the molar crystal's concentration and S is the supersaturation. The term D_{AB} is the diffusivity coefficient calculated to predict it at different operating conditions for temperature and concentration. A commonly expression for this purpose is the Stokes-Einstein equation (Mersmann, 2001):

$$D_{AB} = \frac{kT_{cr}}{2\pi \eta_L d_m} \quad (16)$$

where d_m is the diameter of a molecule whereas η_L is the dynamic viscosity. Another important parameter that considers physical properties from the cane sugar crystals is the surface tension γ_{CL}, defined in Equation (17). The parameter K has a value of 0.414, calculated experimentally by Mersmann (2001).

$$\gamma_{CL} = kT_{cr} K (C_C N_A)^{2/3} \ln\left(\frac{C_C}{C^*} \right) \quad (17)$$

For the crystal growth, cane sugar batch crystallization is dominated by surface integration (Quintana *et al*., 2008), whereby, its mathematical modelling turns out to be more complex thus requiring a model that takes into account both diffusion and integration of limited crystal growth. This works considers the physical model derived by Mersmann (2001) and implemented by Gerstlauer *et al*., (2002):

$$\frac{G}{2k_d(L)} = \underbrace{\frac{\Delta C}{C_C}}_{diffusion} + \underbrace{\frac{k_d(L)}{2k_r C_C} - \sqrt{\left(\frac{k_d(L)}{2k_r C_C} \right)^2 + \frac{k_d(L)}{k_r C_C} \frac{\Delta C}{C_C}}}_{integration} \quad (18)$$

In this equation, k_r is an integration rate constant. Equation (19) calculates the mass transfer coefficient $k_d(L)$.

$$k_d(L) = \frac{D_{AB}}{L} \left[2 + 0.8 \left(\frac{\bar{\varepsilon} L^4}{v_L^3} \right)^{1/5} \left(\frac{v}{D_{AB}} \right)^{1/3} \right] \quad (19)$$

The attrition of crystals due to stirrer collisions is considered next. When a population of crystals has a collision with a stirrer, it produces three different particle number fluxes in the population balances. This can be explained as follows (Gertlauer *et al*. 2002):

1. A particle number flux $\dot{n}_{at}^-$ due to the removal of large original crystals that collide with the stirrer,
2. A particle number flux $\dot{n}_{at,2}^+$ due to the formation of an abraded original cristals with a length somewhat smaller than the original crystals, and,
3. A particle number flux $\dot{n}_{at,1}^+$ due to the formation of a distribution of attrition fragments resulting from the crystal-stirrer collision.

Based on the above, the overall particle number flux due to attrition $n_{at}^{\pm}$, which is considered in Equation (1), can be calculated as follows:

$$n_{at}^{\pm}(L) = -\dot{n}_{at}^-(L) + \dot{n}_{at,2}^+(L) + \dot{n}_{at,1}^+(L) \quad (20)$$

where:

$$\dot{n}_{at}^-(L) = \beta(L) n(L) \quad (21)$$

$$\dot{n}^{+}_{at,2}(L) = \int_{L}^{L_\infty} \delta\left(L - \underbrace{\left[L'^3 - \frac{V_{p,at}(L')}{k_v} \right]^{1/3}}_{\text{Length of crystal after attrition}} \right) \beta(L') n(L') dL' \tag{22}$$

$$\dot{n}^{+}_{at,1}(L) = \int_{L}^{L_\infty} N_{frag}(L') \times [h(L - L_{frag,min}) - h(L - L_{frag,max}(L'))] \times f_{frag}(L, L') \beta(L') n(L') dL' \tag{23}$$

$V_{P,at}(L')$ denotes the abraded volume that a crystal of length L' loses due to crystal-stirrer collision. k_V is the volumetric shape factor, having a value of $\pi/6$ (Beckman, 2004) for a cane sugar crystal, f_{frag} is the size distribution of attrition fragments, N_{frag} is the number of attrition fragments, $L_{frag,min}$ and $L_{frag,max}(L')$ are the minimal and maximal fragment length, respectively.

3.3 Empirical kinetic modelling approach

Empirical models describing the behavior of different crystallization systems have been proposed in the literature (Nagy *et al*., 2003; Quintana *et al*., 2004; Ouiazzane *et al*., 2008). Although they are typically robust in the spanned range, these models need access to accurate experimental data to determine the kinetic parameters through parameter estimation. The simplest empirical expressions involve supersaturation raised to a constant and pre-exponential constant (Qiu and Rasmuson, 1994; Quintana *et al*., 2004). Some variants take into account the agitation rate, the mass of crystals (Quintana *et al*., 2004) and the activation energy (Mitchell *et al*., 2011). Equations (24) - (26) describes the primary nucleation, crystal growth rate and an empirical relationship for the birth and death rates generated by attrition and breakage of crystals, respectively. These expressions have been used in this work because they have been applied to simulate a wide range of operating conditions, e.g., optimal agitation rate under uncertainty (Bolaños *et al*., 2014), compute the metastable zone width (MSZW) (Kobari *et al*., 2010). In addition, these expressions have shown good predictions under a bounded range of operating conditions.

$$B_{hom} = K_b S^b M_T^j N_r^p \tag{24}$$

$$G = K_g S^g N_r^h \tag{25}$$

$$\alpha(L) = K_a S^a M_T^k N_r^r FTM \tag{26}$$

Bolaños (2000) and Quintana *et al*., (2004) developed equation (26) to account for the birth and the death rates of the crystals. This expression aims to measure the general effect of the breakage and attrition of crystals. In Equations (24) and (26), the term M_T denotes the total mass of crystals, defined as follows:

$$M_T = \rho_c k_V \int_0^{L_\infty} F(L,t) L^3 dL \tag{27}$$

3.4 Physicochemical properties

Equation (28) is a well-known density relationship proposed by Mersmann (2001), which make use of the data reported by Swindells *et al*., (1958) to calculate the viscosity of the sucrose-water solution in a range from 20% to 75% of sucrose mass and temperatures from 40 to 80 °C. This work uses such equation to estimate the solution's density in the water.

$$\rho_{Liq} = \frac{1 + \frac{M_c}{M_{Liq}^0}}{1 + \left(\frac{\rho_{Liq}^0}{\rho_c} \right) \frac{M_c}{M_{Liq}^0}} \tag{28}$$

where ρ_{Liq}^0 is the density of water, ρ_c is the density of crystals, M_{Liq}^0 is the mass of solvent and M_c is the mass of crystals. Equation (29) gives the saturation concentration of sucrose C_{sat}, (Ouiazzane *et al*. 2008), in terms of weight of dry substance (w_{DS}) (Equation 30).

$$C_{sat} = \frac{w_{DS}}{100 - w_{DS}} \tag{29}$$

$$w_{DS} = 64.47 + 0.10336 T_{cr} + 14.20 \times 10^{-4} T^2 - 70.20 \times 10^{-7} T^3 \tag{30}$$

Table 2 lists the physical properties of sucrose and water. Velazquez *et al*., (2010) have reported the geometric properties of the crystallizer. For further information on physicochemical and geometrical properties on this system, the readers are referred to Gahn and Mersmann (1999a, 1999b), Ploβ and Mersmann (1989) and Gerstlauer *et al*., (2002).

3.5 Parameter estimation

The mechanistic framework requires of physical constants, i.e. k_r and Γ, to fully specify the model.

Table 2. System's physical properties

Parameter	Value	Units	References
n_{LA0}	19.21	mol	—-
n_{L0}	132.2	mol	—-
k_v	$\pi/6$	adim	Beckman (1994)
Hv	645×10^{6}	Pa	Duncan (1989)
V	0.31	adim	Leigh (1967)
E	32.3×10^{9}	Pa	Duncan (1989)
M_a	0.342	kg/mol	Green & Perry (2007)
M_b	0.018	kg/mol	Green & Perry (2007)
Na	6.023×10^{23}	1/mol	Gahn & Mersmann (1999a)
K_b	1.38×10^{-23}	J/K	Gahn & Mersmann (1999a)
R	8.3145	J/(K mol)	Gahn & Mersmann (1999a)
ρ_s	1588	kg/m3	Green and Perry (2007)
Cp_w	586.2	J/(kg K)	Bolaños *et al*., (2014)
Cp_s	2468.7	J/ (kg K)	Bolaños *et al*., (2014)
T_0	70	°C	Bolaños *et al*., (2008)
A_1	0.2004	m^2	Bolaños *et al*., (2014)
α_v	0.27	adim	Marek *et al*., (2001)

Kalbasenka *et al*., (2011) determined these constants through parameter estimation by optimization from experimental data generated under different operating conditions. These constants are related to attrition phenomena and crystal growth and have a clear physical meaning: surface related energy increase Γ_S and the integration rate constant for crystal growth k_r. Gerstlauer *et al*., (2002) included a constant related to primary nucleation rate C_{het}, which represents the heterogeneity degree of primary nucleation. The present study formulates a least-squares optimization problem to determine those constants, i.e.

$$\min \varnothing(\Gamma_s, k_r, C_{het}) = w_1 \sum_{i=1}^{N}\left(\frac{M_{T,i}^{cal}-M_{T,i}^{exp}}{M_{T,i}^{exp}}\right)^2 + w_2 \sum_{i=1}^{N}\left(\frac{D(4,3)_i^{cal}-D(4,3)_i^{exp}}{D(4,3)_i^{exp}}\right)^2 + w_3 \sum_{i=1}^{N}\left(\frac{\rho_i^{cal}-\rho_i^{exp}}{\rho_i^{exp}}\right)^2 \quad (31)$$

where, $M_{T,i}^{cal}$, $D(4,3)_i^{cal}$ and ρ_i^{cal} represent the mass of crystal in kg, average diameter of crystal (μm) in % Volume, and continuous phase density (m^3/kg) at each sampling time (i) i.e. 15 min, 30 min, 45 min, 60 min, 75 min and 90 min, respectively; whereas w_n is a weight assigned to each term in the penalty function and used to uniformly weight each contribution. On the other hand, the empirical model requires eleven parameters: a, b, g, h, j, k, k_a, k_b, k_g, p and r, which need to be determined by the same procedure. The initial values used in the present analysis were taken from Quintana *et al*. (2008) for seeded batch crystallization of cane sugar. To solve problem (31), this work employed the constrained nonlinear programming function (*fmincon*) available in MATLAB. To ensure degrees of freedom in the analysis, each experiment (100, 300 and 600 rpm) was done three times, getting 54 measurements to estimate 11 parameters.

It is well known that the dynamic mathematical model of a batch crystallizer is highly nonlinear (Bolaños *et al*., 2014). To address that issue, problem (19) uses the *multistart* built-in function available in MATLAB with twenty randomly bounded initial values. This was done to improve parameter estimation

from problem (31) by minimizing the error between the data generated by the simulation and experimental data at different agitation rates.

3.6 Population balance solution

The PBE was solved by applying a first order centered finite difference for the L domain, from L_{min} = 1 μm to L_{min} = 801 μm with a spacing of ΔL = 10 μm where $\Delta L = L_i - L_{i-1}$. Thus, a set of 80 ODEs for each step in the time defines the entire L domain. Significant differences between the mechanistic and the empirical models exist. While the mechanistic model accounts for variations in the crystal growth rate as a function of the characteristic length, empirical models assume that this rate is constant regardless characteristic crystal length. The term $\alpha(L_i)$ describes the rate of appearance and disappearance of crystals for the empirical framework. Nevertheless, secondary nucleation through attrition replaces the $\alpha(L_i)$ term in the mechanistic framework. This results in the implementation of different discretization schemes by centered finite difference for each approach as shown in Equations (32) and (33). The solution of the full mathematical framework uses the *ode15s* function available in MATLAB, which implements the backward differentiation formulas (also known as Gear's method).

$$\frac{dn(L_i,t)}{dt} = \frac{Gn(L_{i+1},t) - Gn(L_{i-1},t)}{2\Delta L} + n(L_i,t)^{+}_{nu} + n(L_i,t)^{\pm}_{att} \tag{32}$$

$$\frac{dn(L_i,t)}{dt} = \frac{Gn(L_{i+1},t) - Gn(L_{i-1},t)}{2\Delta L} + n(L_i,t)^{+}_{nu} + \alpha(L_i) \tag{33}$$

3.7 Modelling assumptions

To simplify the mathematical model, the following assumptions were considered:

- Negligible agglomeration crystals.
- Crystal nuclei produced have negligible size.
- The system is well mixed.
- The crystals inside the tank are well suspended, i.e., no accumulation of crystals at the bottom of the crystallizer.

3.8 Seed's CSD

Equation (2) and (3) lists the initial and boundary conditions for the PBE considered in this work.

Table 3. Seed's characteristics

Range (m)	$165^{-6} - 222^{-6}$
Mass (kg)	0.005
λ_i	7.842×10^5
$S(4,3)_{seed}$ (m)	19.52×10^{-6}
$D(4,3)_{seed}(m)$	$195.26 \times 10{-}6$

The seeded crystals were obtained from commercial cane sugar $D(4,3)$ = 450 − 550 μm with high purity concentration, which was crushed and then classified using sieves of size 150 μm, 180 μm and 212 μm (sieves No. 70, 80 & 100 according with the American Standard Test Sieve Series (ASTM)). Crystals retained in the sieve of 180 μm were selected. The CSD approximates to a normal distribution using Equation (34) (Hermanto *et al.*, 2008). Table 3 includes the required parameters needed to solve Equation (34).

$$F(L,0) = F_{seed,i}(L,0) = \frac{\lambda_i}{\sqrt{2\pi}\sigma_{seed}} \exp\left(-\frac{(L-\mu_{seed})^2}{2\sigma^2_{seed}}\right) \tag{34}$$

4 Results and discussion

4.1 Temperature profile

In the first experimental test, the vacuum pressure was set to 76.20 kPa producing a suddenly change in temperature from 70 °C to 58 °C within the first 10 minutes. This sudden decrease in temperature is attributed to the fast increase in vacuum pressure from 0 kPa to 76.20 kPa (air extraction), where the system reaches the thermodynamic equilibrium. After 40 minutes of this process, the system reaches a vacuum pressure of 86.66 kPa, and generates a natural cooling profile. The trajectory described for both cooling stages are different mainly due to the vacuum pump. At the beginning, the vacuum pump reaches 76.20 kPa due to the great amount of air inside the crystallizer but after 40 minutes, the system takes a longer time to reach 86.66 kPa (water steam) thus producing a trajectory that follows a natural profile. Supersaturation controls these programmed paths to keep the concentration close to solubility curve (Equation 28). Figure 2 shows that the predicted profile for both approaches, i.e. empirical (TPL) and mechanistic. As shown in this figure, the models describe adequately the temperature trajectory with respect to experimental data.

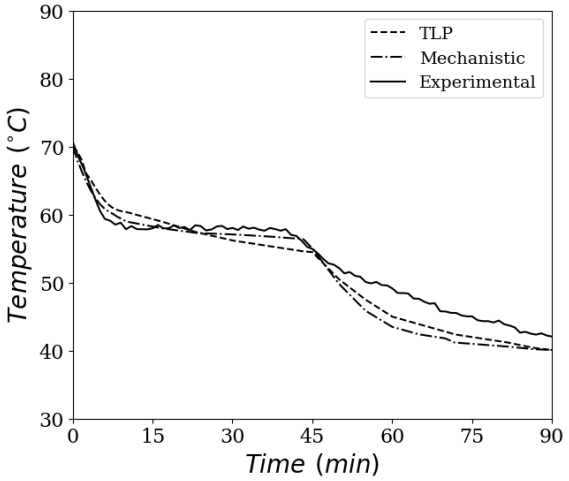

Fig. 2. Temperature profile validation for mechanistic and TPL approach.

Note that the cooling stage (40 - 90 min) presents minor deviations. A deep analysis of the experimental set-up shows that the vacuum generation system has a time delay, which was not included in the present mathematical framework. Both modelling approaches take into account the changes in vacuum pressure, reflecting changes in the temperature, increasing the prediction capabilities.

4.2 Concentration profile

Phenomena such as primary and secondary nucleation affects the solute concentration as described below. Solution´s concentration needs to reach the metastable zone to form embryos of critical size L_{crit} (Mersmann, 2001), which grow as long as there is dissolved solute available (Jones, 2002). On the other hand, attrition and breakage produce smaller crystals that limit the growth of the early formed crystals since they have to compete for the dissolved solute. Figures 3a - 3c shows the experimental data and the predicted concentration profiles generated from Eq. (4) by using the empirical (TPL) and mechanistic modelling approaches at 100, 300 and 600 rpm, respectively.

Major deviations of the mechanistic approach from the experimental data are evident for all the experiments. This lack of fitting can be attributed to the to the diffusion-integration growth mechanism that dominates the cane sugar crystallization (Quintana *et al.*, 2008), generating lower mass transfer of dissolved solute to crystals faces than the predicted for the mechanistic approach.

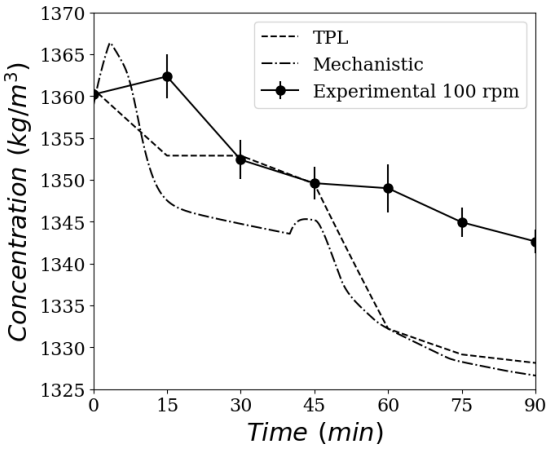

a)

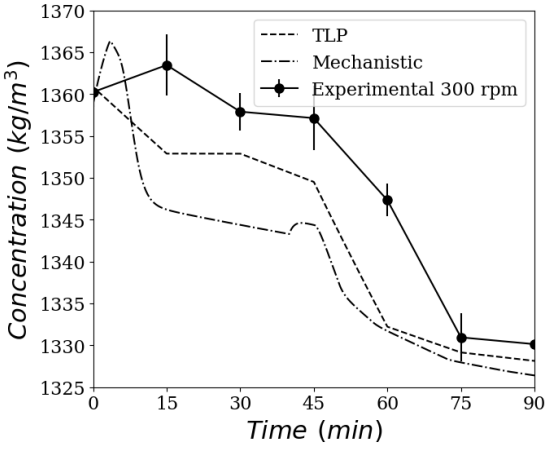

b)

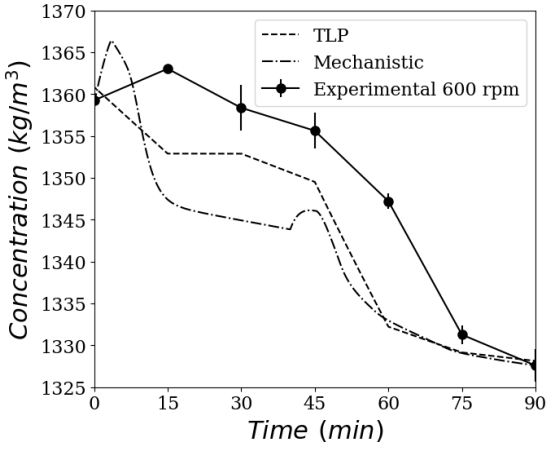

c)

Fig. 3. Concentration profile for agitation rate: a) 100 rpm, b) 300 rpm and c) 600 rpm

Table 4. Concentration errors (ε)

Agitation rate	Mechanistic	TLP
100 rpm	7.76%	3.27%
300 rpm	4.98%	3.18%
600 rpm	4.09%	3.05%

However, empirical models (TPL) fit better than mechanistic approach due to the use of estimated parameters. The use of different agitation rates produces variations in the concentration (see Figures 3a - 3c) due to the increase in mass transport of dissolved solute to crystals faces and the effect that on the solvent evaporation rate.

Moreover, the mechanistic approach can capture the increase in concentration due to the evaporation of solvent at the beginning of process (0 - 10 min). This is explained as follows: as the solvent is evaporated, the concentration reach the metastable zone (nucleation), then, concentration is decreased again due to the mass transfer from the dissolved solute towards the crystals. On the other hand, the empirical approach (TPL) only captures the decrease in concentration. This result is remarkable, while there is a recent interest in the dynamic regulation for the cooling temperature trajectory applied to a batch system with the aim to reduce the crystals formed from undesired nucleation rate (Seki & Su, 2015), being the mechanistic approach the most suitable alternative to handle this kind of control approaches.

Table 4 presents the errors by using Eq. (25) for each modelling approach against experimental data. Both approaches have major deviations at low agitation rate (i.e. 100 rpm). For 300 and 600 rpm, both approaches show acceptable errors. From this section, the results show that the empirical approach (TPL) has better kinetic modelling predictions to represent the experimental concentration.

$$\varepsilon = 100 \cdot \sum_{i=1}^{n} \left(\frac{C_{exp} - C_{sim}}{C_{exp}} \right)^2 \qquad (35)$$

4.3 *Crystallization kinetics*

The constants obtained by applying the procedure described in Section 3.5 are $k_r = 9.1 \times 10^{-4}$ (m^4 / mol s), $\Gamma s = 1.38 \times 10^{-6}$ (J m / mol) and $C_{het} = 0.8$. This is the first work that reports data estimation for the mechanistic modelling approach for cane sugar batch crystallization; hence, a comparison against previous work is not available.

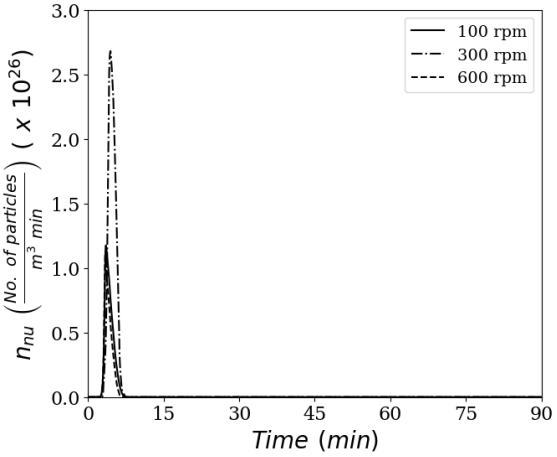

Fig. 4. Primary nucleation from mechanistic approach under 100, 300 and 600 rpm.

Opposed to the mechanistic approach, there are available experimental data reported for empirical kinetic approach (Quintana *et al*., 2004, Quintana *et al*., 2008, Bolaños *et al*., 2014). Table 5 presents the results obtained in this work and a comparison with data reported by Quintana *et al*., (2008) and Bolaños *et al*., (2014). As reported in Quintana *et al*., (2004), each set of operating conditions has specific kinetic parameters, hence we expect differences between the data reported previously and that obtained in this work, due to both data were obtained at different vacuum pressures and cooling temperature trajectories.

4.3.1 *Primary nucleation*

The primary nucleation affects the CSD due to the increase in population of crystals with a length close to L_{crit}. Although this phenomenon can occur during the evolution of this process, it takes place just when the supersaturation (S_r) reaches the metastable zone. The mechanistic approach (Eq. 15) well describes this behavior (see Figure 4) where a pulse response denotes the primary nucleation with three agitation rates, which only takes place early in process, i.e. within the first 15 min of the batch. Figure 5 shows the primary nucleation for the empirical model (TPL) as a continuous and ascendant dynamic response to the same agitation rates.

As previously mentioned, Figures 4 and 5 have different dynamic responses, mainly due to the differences in the mathematical formulation for each modelling approach.

Table 5. Empirical kinetic parameters

Primary homogeneous nucleation			
Parameter	Adjusted value	Quintana *et al.*, (2008)	Bolaños *et al.*, (2014)
$k_b \left[\frac{\#\ crystals}{cm^3 \cdot \min \cdot (g\ cm^3)^j \cdot (rpm)^p}\right]$	23.00	10.50	1.56×10^{-2}
b	2.80	5.03×10^{-3}	6.27×10^{-4}
j	5.00×10^{-4}	5.00×10^{-4}	2.04×10^{-3}
p	4.20×10^{-3}	3.50×10^{-2}	1.41

Crystal growth			
Parameter	Adjusted value	Quintana *et al.*, (2008)	Bolaños *et al.*, (2014)
$k_g \left[\frac{cm}{\min \cdot (rpm)^h}\right]$	2.00×10^{-1}	7.50×10^{-4}	1.31×10^{-5}
g	1.05	1.05	1.03
h	3.29×10^{-2}	6.24×10^{-1}	8.45×10^{-1}

Crystal death and birth			
Parameter	Adjusted value	Quintana *et al.*, (2008)	Bolaños *et al.*, (2014)
$k_a \left[\frac{\#\ crystals}{cm^3 \cdot (g\ cm^3)^k \cdot (rpm)^r}\right]$	1.00×10^{-3}	1.00	----
a	1.10	7.00×10^{-2}	----
k	9.00×10^{-2}	2.50×10^{-2}	----
r	1.00×10^{-2}	1.00×10^{-3}	----

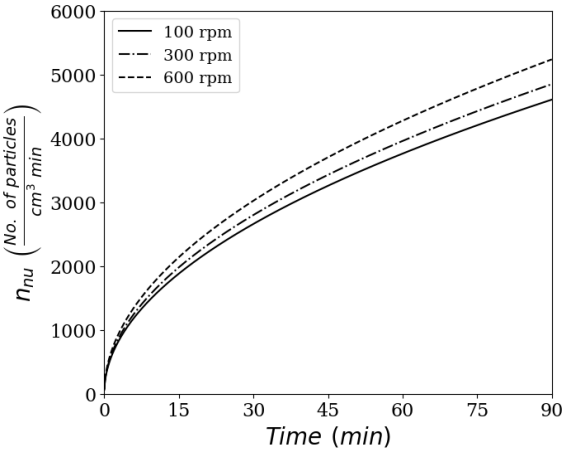

Fig. 5. Primary nucleation from TLP approach under 100, 300 and 600 rpm.

The mechanistic approach (Figure 4 and Eq. (15)) satisfies the phenomenological behavior observed experimentally reported in Bolaños *et al*. (2014). By analyzing Figures 3a - 3c, during the time interval from 0 to 10 min, an increase in concentration occurs (due to solvent evaporation); this makes the concentration to reach the nucleation zone. After 10 min, concentration presents a downward trend, decreasing the concentration towards the growth zone where theoretically should not appear homogeneous primary nucleation. Related with the agitation rate, 100 rpm and 600 rpm has the same nucleation rate: 2.0×10^6 (No. of particle / m^3 min), opposed with the case with 300 rpm, where the pulse response reach values for 2.7×10^6 (No. of particle / m^3 min). Experimentally, these results are explained as follows: for low agitation rates (100 rpm), the concentration is not uniform inside the crystallizer allowing the presence of micro-volumes (ΔV), where only some of them have the concentration needed to generate nucleation, decreasing the global nucleation rate. For the case of high agitation rate (600 rpm), the minimum size of a nuclei (L_{crit}) increase, avoiding the early formation of new crystals.

Prediction for primary nucleation rate by using TPL approach shows an increasing trend. Due to the mathematical formulation (see Eq. 24), supersaturation has a strong effect at the beginning of the process, where high values of supersaturation are reached due to the evaporation of solvent. Then, after supersaturation go downwards; the increment of nucleation rate promotes the formation of new particles, according to Eq. (24), nucleation rate depends on mass of crystals which increases during all process and produces different nucleation rates at the end of process.

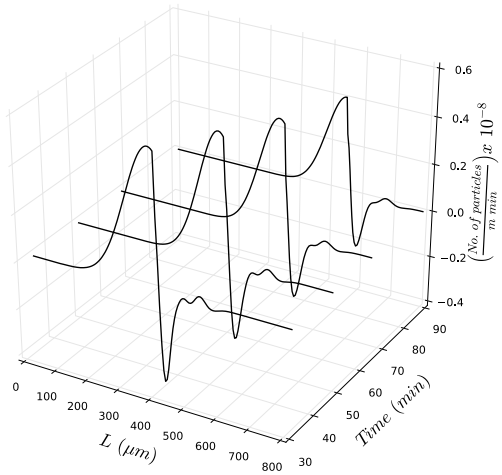

a)

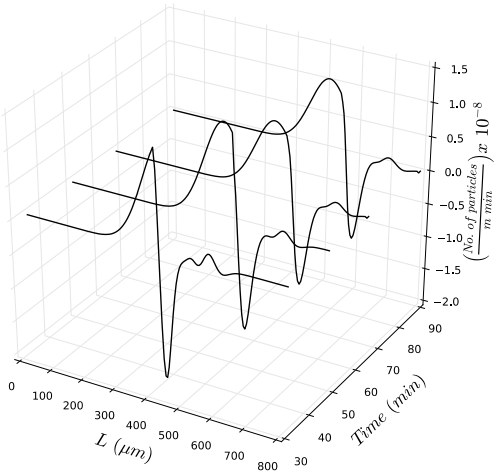

b)

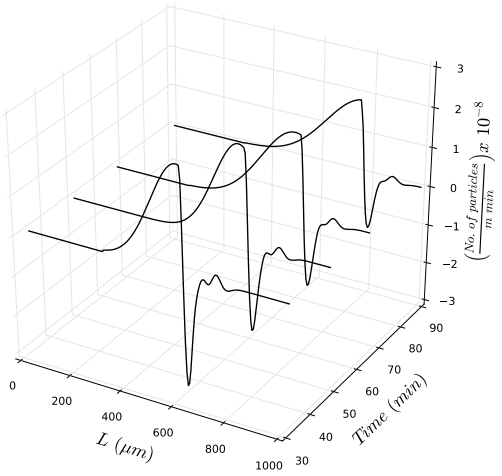

c)

Fig. 6. Overall particle flux number due to attrition at: a) 100 rpm, b) 300 rpm and c) 600 rpm.

Figure 5 shows the three nucleation rates predicted by Eq. (24), getting final values of 4,607.71, 4,849.97 and 5,237.96 No. of particles/cm^3 min for 100, 300 and 600 rpm, respectively.

4.3.2 Secondary nucleation

Figures 6a - 6c shows the variation of the characteristic length (L) of the abraded crystals at agitation rate of 100 rpm, 300 rpm and 600 rpm, resulting from Eq. (20). The population (z axes) represents the particle number of abraded original crystals and the particle number of generated crystals somewhat smaller than the original crystal and the crystals abraded. The mechanistic framework predicts an increase in the overall particle flux number given that attrition is proportional to the characteristic crystal length. Thus, the attrition phenomena have a stronger effect into crystals greater than 350 μm, 400 μm and 550 μm for 100 rpm, 300 rpm and 600 rpm, respectively, showing a sharp decreasing in the overall flux number. However, by population balance (Eq. 32), at different L intervals, particles can be lost for attrition (death crystals) producing negative values in the overall flux number (sharp decreasing) if there are not particles going in the L interval. This is observed in Figures 6a - 6e when the crystal lengths reach 400 - 600 μm (at different times).

Nowadays, it is not possible to validate the predicted values by the mechanistic model due to the lack of experimental data and the difficulty in measuring the abraded crystal size online.

4.3.3 Crystal growth rate

Figure 7 shows the results for crystal growth rate from the mechanistic approach (Eq. 18). It is clear how agitation rate affects the growth of crystals. 600 rpm promotes faster growth at 20 min of process (In this time, the process arises the maximum relative supersaturation) compared to 100 and 300 rpm. Towards the end of the process, crystal growth rate should reach a zero value (thermodynamic equilibrium); the three agitation rates allow the crystal growth rate to reach values close to zero, where the value of 600 rpm again predicts better values (close to 0) compared to 100 and 300 rpm.

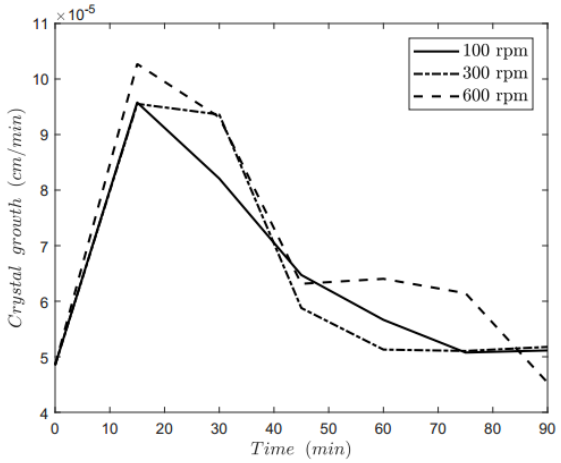

Fig. 7. Crystal growth from mechanistic approach under 100, 300 and 600 rpm.

4.4 Average crystal diameter D(4,3)

Figures 8a - 8c show that the mechanistic model predicts a peak on the D(4,3)'s path around the 6 minute for the experiments conducted at the three different agitation rates. This can be explained as follows: the seed fed grows without any generation of new nuclei until, by effect of solvent evaporation, saturated solutions achieve the metastable limit for growth zone. Once completed, the primary nucleation phenomena take place (see Figure 4). These new nuclei of length Lcrit reduce the average crystal diameter D(4.3). Empirical models do not predict such exhibited behavior in the evolution of the D(4,3) (Figures 8a-8c).

In the case of an agitation rate of 100 rpm, mechanistic and empirical approaches follow the same behavior with coefficients of determination (R^2) of 0.95 and 0.94, respectively; as it is shown in Figure 8a.

For a constant agitation rate of 300 rpm the R^2 are 0.98 and 0.95 for the mechanistic and empirical models, respectively (see Figure 8b). Regarding the results for an agitation rate of 600 rpm (see Figure 8c), an R^2 of 0.80 is obtained for empirical models. On the other hand, mechanistic models follow the behavior observed from the experimental data. According to Mersmann *et al*., (2002), the generated fragments by attrition is proportional to the dynamic pressure of the crystallizer, which increases as the square of the tangential velocity of the agitator and the particle density.

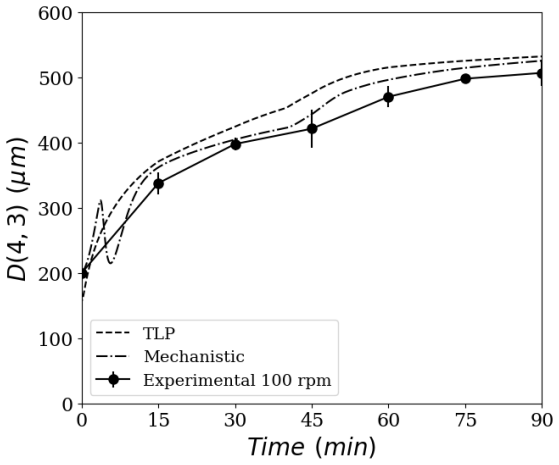

a)

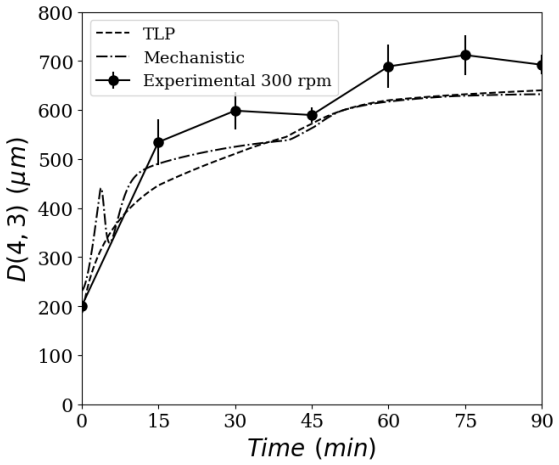

b)

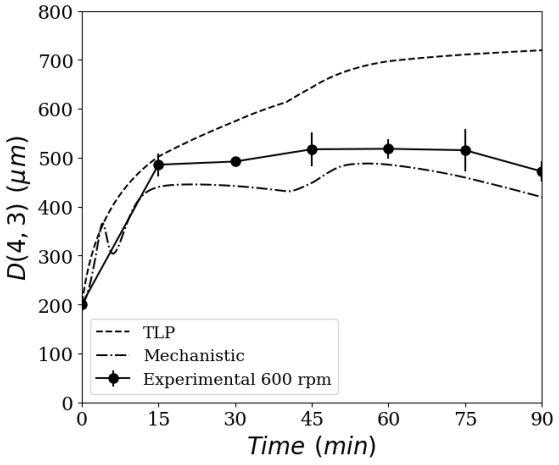

c)

Fig. 8. D(4,3) for: a) 100 rpm, b) 300 rpm and c) 600 rpm.

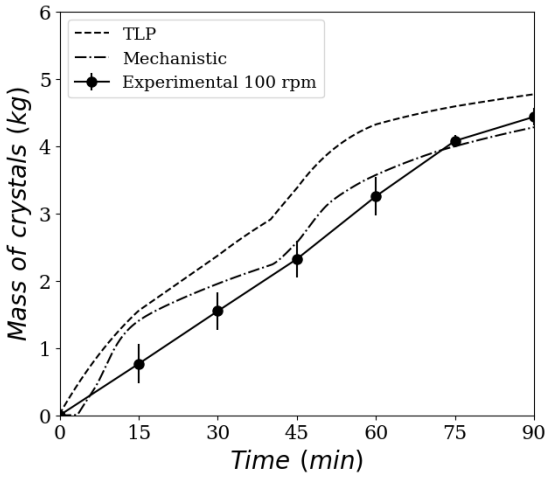

a)

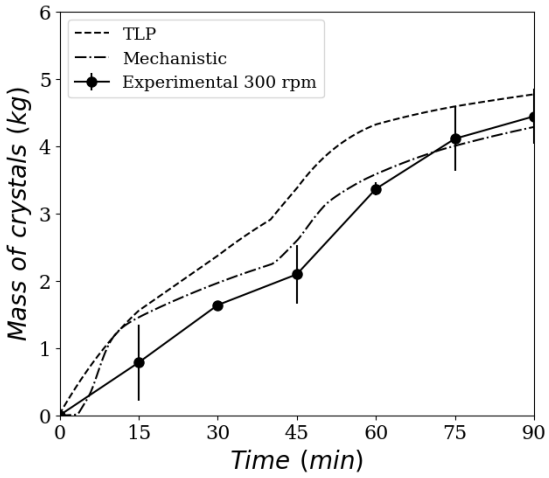

b)

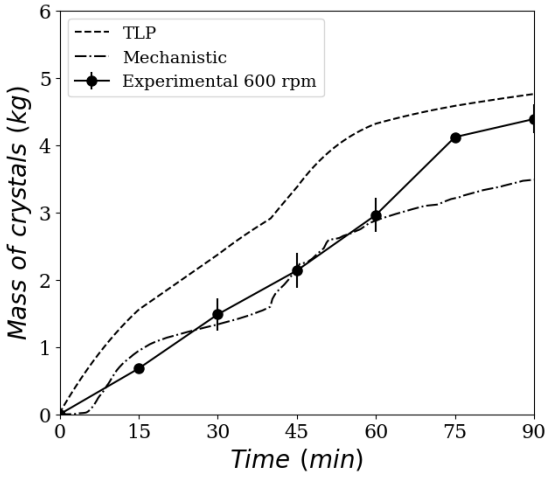

c)

Fig. 9. Mass of crystals for: a) 100 rpm, b) 300 rpm and c) 600 rpm.

The mechanistic framework describes this phenomenological behavior in detail. Hence, the capable of prediction of these models is more accurate for crystallization processes where secondary nucleation occurs (Kalbasenka *et al*., 2011).

4.5 Mass of crystals

Figures 9a-9c show the mass of crystals at the three different agitation rates studied in this work. The empirical model returned R^2 of 0.92, 0.92, and 0.91 (when compared to the experimental data) for 100 rpm, 300 rpm and 600 rpm, respectively. Similarly, mechanistic models have R^2 of 0.96, 0.94 and 0.95. Figures 9a-9c also show that there are no significant variations in the amount of mass of crystals at the end of the batch; Akrap *et al*., (2010) and Bolaños *et al*., (2014) reported that the agitation rate and profiles do not affect the mass of crystals during the batch.

From the results, mechanistic approach allows a better representation of experimental data and should be applied for accurate simulation of cane sugar crystallization. In the case of the TPL approach, results show minor deviations compared with experimental data, with the advantage of easy solution where no physicochemical properties are needed to solve it, property with use in model-based (dynamic) optimization.

Conclusions

This work presented an analysis between empirical and mechanistic approaches of kinetics for vacuum batch crystallization of cane sugar. Unlike the empirical approach, the mechanistic model predicts the expected behavior for the primary nucleation, following a pulse response. Primary nucleation should not occur throughout the process if temperature profiles drive the solute concentration. However, both approaches fail at describing the continuous phase density. The empirical approach is not adequate to predict nucleation rates when working with different operating conditions for which the kinetic parameters were originally adjusted (temperature, vacuum pressure and agitation speed). The secondary nucleation rate is predicted adequately only by the mechanistic approach, since it generates satisfactory information on the size of crystals (L) that loose from mechanical effects, and crystals that are born by attrition (fragments). This approach represents a better

option than the TPL for inclusion in the population balance equation and its solution by method of lines.

The growth rate of crystals must be adequately calculated, since it is the basis of the prediction of the average crystal size in %volume D(4,3). The formulated mechanistic approach considers the diffusion-integration mechanism and allows a good correlated prediction with the solution´s concentration.

The kinetic constants obtained for the mechanistic and empirical models have similar orders of magnitude compared to those reported in previous studies. In the cases of agitation rates of 100 rpm and 300 rpm, it is shown that both approaches have higher coefficients of determination than 0.9 for the D(4,3) and mass of crystals. In the case for 600 rpm, the discrepancies observed in the empirical model in the D(4,3) can be attributed to the attrition phenomena, which is not accurately captured by the term of birth and death of crystals.

Finally, from the results of both approaches and experimental validation, we conclude that mechanistic approach best represents the dynamic behavior of cane sugar batch crystallization under different operational conditions than the empirical approach (TPL).

Acknowledgements

The authors would like to acknowledge the support of the National Council of Science and Technology (CONACyT) for the financing granted to this project and the international scholarship provided to the student of the Master's Degree in Sciences in Chemical Engineering Lazaro Elioenai Hernandez Ariza. In addition, the authors would like to acknowledge the Emerging Leaders in the Americas Program (Canada) for the funding provided.

Nomenclature

A_{cool}	heat transfer area, m
B_{nu}	primary nucleation rate, 1/ m^3 s
C	molar concentration, kmol/ m^3
C^*	saturation molar concentration, kmol/ m^3
C_C	crystal molar concentration, kmol/ m^3
C_{exp}	experimental concentration, kg/m^3
C_{sim}	simulated concentration, kg/ m^3
C_p	heat capacity, kJ/kg
d_m	molecule diameter, m
D(4,3)	average diameter in % volume, m
D_{AB}	diffusion coefficient, m^2/s
dL	change in crystal length, m
dv	change in crystal growth rate, m/s
∂G	change in total enthalpy
G	growth rate of individual crystal, m/s
k	Boltzmann constant, 1.381×10^{-23} J/K
k_r	integration rate constant
k_V	volume shape factor, dimensionless
k_d	mass transfer coefficient for crystal growth, m/s
K	factor, dimensionless
L	crystal length, m
L_{frag}	fragment length, m
M_w	molecular weight, kmol
M_T	total mass of crystals, kg
N_A	Avogadro's number, 6.023×10^{26}kmol^{-1}
N	number density function, 1/m
$n_{at}^{\pm}$	individual particle number fluxes due to attrition at the stirrer, 1/m s
n_{cool}	cool water rate, m
n_{gr}, n_{nu}	molar fluxes between liquid phase and solid phase due to growth and primary nucleation, mol/s
n_{liq}	total number of moles in the liquid phase, mol
n_{vap}	evaporation flux, kg
p_l	liquid pressure, kPa
p_V	vapor pressure, kPa
R	gas constant, J/mol K
S_r	supersaturation ratio, dimensionless
S(4,3)	standard deviation in % volume, μm
t	time, min
T_{cr}	absolute temperature of the crystallizer, K
V_{liq}	volume of liquid phase, m^3
$V_{P,at}$	abraded volume of crystals, m^3
v	stoichiometric coefficient
w_{DS}	weight of dry substance, Brix

Greek symbols

ε	error, dimensionless
$\overline{\varepsilon}$	specific energy dissipation rate of stirrer, W/kg
α_V	adhesion coefficient
β	attrition rate, 1/s
η_L	dynamic viscosity, Pa·s

γ_{CL}	interfacial tension, J/m^2
σ	relative supersaturation, dimensionless
ρ_{liq}	density of liquid phase, kg/m^3
ρ_s	density of solid phase, kg/m^3

References

Akrap, M., Kuzmanić, N., & Prlić-Kardum, J. (2010). Effect of mixing on the crystal size distribution of borax decahydrate in a batch cooling crystallizer. *Journal of Crystal Growth 312*, 3603-3608.

Beckman, J. R. (1994). *Handbook of Chemical Engineering Calculations*. McGraw-Hill, New York.

Bermingham, S. K., Neumann, A. M., Kramer, H. J., Verheijen, P. J., Van Rosmalen, G. M., & Grievink, J. (2000). A design procedure and predictive models for solution crystallization processes. *Fifth International conference on Foundations of Computer-Aided Process Design*, 250-264.

Besenhard, M. O., Chaudhury, A., Vetter, T., Ramachandran, R., & Khinast, J. G. (2015). Evaluation of parameter estimation methods for crystallization processes modeled *via* population balance equations. *Chemical Engineering Research and Design 94*, 275-289.

Bolaños, E. R. Control and optimization of operating conditions from cooling batch crystallizers. (2000). Ph.D. Thesis, I.T. de Celaya, México.

Bolaños, R. E., Xaca, X. O., Alvarez, R. J., Lopez, Z. L. (2008). Effect analysis from dynamic regulation of vacuum pressure in an adiabatic batch crystallizer using data and image acquisition. *Industrial and Engineering Chemistry Research 47*, 9426-9436.

Bolaños, R. E., Sánchez, S. K. B., Urrea, G. R., Ricardez S. L. (2014). Dynamic modelling and optimization of batch crystallization of cane sugar under uncertainty. *Industrial & Engineering Chemistry Research 53*, 13180-13194.

Choong, K. L; Smith, R. (2004). Optimization of batch cooling crystallization. *Chemical Engineering Science 59*, 313-327.

Duncan, H. W. C., Weatherly, G. C. (1989). Evaluating the hardness, Young's modulus and fracture toughness of some pharmaceutical crystals using microindentation techniques. *Journal of Materials Science Letters 8*, 1350-1352.

Gahn, C., & Mersmann, A. (1999a). Brittle fracture in crystallization processes Part A. Attrition and abrasion of brittle solids. *Chemical Engineering Science 54*, 1273-1282.

Gahn, C., & Mersmann, A. (1999b). Brittle fracture in crystallization processes Part B. Growth of fragments and scale-up of suspension crystallizers. *Chemical Engineering Science 54*, 1283-1292.

Gerstlauer, A., Motz, S., Mitrović, A., & Gilles, E. D. (2002). Development, analysis and validation of population models for continuous and batch crystallizers. *Chemical Engineering Science 57*, 4311-4327.

Green, D., Perry, R. (2007). *Perry's Chemical Engineering Handbook*. McGraw Hill Education, Eighth Edition.

Hermanto, M. W., Kee, N. C., Tan, R. B., Chiu, M. S., & Braatz, R. D. (2008). Robust Bayesian estimation of kinetics for the polymorphic transformation of L-glutamic acid crystals. *AIChE Journal 54*, 3248-3259.

Jones, G. A. (2002). *Crystallization Process Systems*. Butterworth-Heinemann.

Kalbasenka, A., Huesman, A., & Kramer, H. (2011). Modelling batch crystallization processes: Assumption verification and improvement of the parameter estimation quality through empirical experiment design. *Chemical Engineering Science 66*, 4867-4877.

Kobari, M., Kubota, N. Hirasawa, I. (2010). Simulation of metastable zone width and induction time for a seeded aqueous solution of potassium sulfate. *Journal of Crystal Growth 312*, 2734-2739.

Leigh, S., Carless, J. E., Burt, B. W. (1967). Compression characteristics of some pharmaceutical materials. *Journal of Pharmaceutical Sciences 56*, 888-892.

Ma, D. L., Tafti, D. K., & Braatz, R. D. (2002). High-resolution simulation of multidimensional crystal growth. *Industrial & Engineering Chemistry Research 41*, 6217-6223.

Marek, R., Straub, J. (2001). Analysis of the evaporation coefficient and the condensation coefficient of water. *International Journal of Heat and Mass Transfer 44*, 39-53.

Mersmann, A. (2001). *Crystallization Technology Handbook*. Second Edition, Marcel Dekker, Inc.

Ali Mesbah, Herman J. M. Kramer, Adrei E. M. Huesman, Paul. J. Van den Hof. (2009). A control oriented stury on the numerical solution of the population balance equation for crystallization processes. *Chemical Engineering Science 64*, 4262-4277.

Mitchell, N. A., Ó'Ciardhá, C. T., Frawley, P. J. (2011). Estimation of the growth kinetics for the cooling crystallization of paracetamol and ethanol solutions. *Journal of Crystal Growth 328*, 39-49.

Motz, S., Mitrović, A., & Gilles, E. D. (2002). Comparison of numerical methods for the simulation of dispersed phase systems. *Chemical Engineering Science 57*, 4329-4344.

Nagy, Z. K., & Braatz, R. D. (2003). Worst-case and distributional robustness analysis of finite-time control trajectories for nonlinear distributed parameter systems. *Control Systems Technology, IEEE Transactions on 11*, 694-704.

Nagy, Z. K., Fevotte, G., Kramer, H., & Simon, L. L. (2013). Recent advances in the monitoring, modelling and control of crystallization systems. *Chemical Engineering Research and Design 91*, 1903-1922.

Ouiazzane, S., Messnaoui, B., Abderafi, S., Wouters, J., & Bounahmidi, T. (2008). Estimation of sucrose crystallization kinetics from batch crystallizer data. *Journal of Crystal Growth 310*, 798-803.

Ploβ, R., & Mersmann, A. (1989). A new model of the effect of stirring intensity on the rate of secondary nucleation. *Chemical Engineering & Technology 12*, 137-146.

Qiu, Y., Rasmuson, Å. C. (1994). Estimation of crystallization kinetics from batch cooling experiments. *AIChE Journal 40*, 799-812.

Quintana, H. P. A., Uribe, M. B., Rico, R. V., Bolaños, R. E. (2008). Comparative analysis of power law type and diffusion-integration kinetic equations in batch cooling of cane sugar. *Revista Mexicana de Ingeniería Química 7*, 171-182.

Quintana, P. H., Bolaños, E. R., Miranda, B. C., Salcedo, L. E. (2004). Mathematical modelling and kinetic parameter estimation in batch crystallization. *AIChE Journal 50*, 1407-1417.

Ramkrishna, D. (2000). *Population Balances: Theory and Applications to Particulate Systems in Engineering*, Academic Press, Inc.

Randolph, A. D., & Larson, M. A. (1988). *Theory of Particulate Processes*. Second Edition. Academic Press, Inc.

Samad, N. A. F. A., Sin, G., Gernaey, K. V., Gani, R. Introducing uncertainty analysis of nucleation and crystal growth models in process analytical technology (PAT) system design of crystallization processes. *European Journal of Pharmaceutics and Biopharmaceutics 85*, 911-929.

Seki, H. Su, Y. (2015). Robust optimal temperature swing operations for size control of seeded batch cooling crystallization. *Chemical Engineering Science 133*, 16-23.

Solomon, C.; Breckon, T. (2011). *Fundamentals of Digital Processing. A Practical Approach with Examples in MATLAB*, First Edition, Jonh Wiley & Sons, Ltd.

Swindells, J. F., Snyder, C. F., Hardy, R. C., Golden, P. E. (1958). Viscosities of sucrose at various temperatures: tables of recalculated values. United States Department of Commerce, National Bureau of Standards.

Velazquez-Camilo, O., Bolaños-Reynoso, E., Rodriguez, E., & Alvarez-Ramirez, J. (2010). Characterization of cane sugar crystallization using image fractal analysis. *Journal of Food Engineering 100*, 77-84.

Westhoff, G. M., Kramer, H. J. M. (2012). Scale-up of suspension crystallisers using a predictive model framework. *Chemical Engineering Science 77*, 26-34.